Estimation of frequency response functions using independant source characterization

D. Ocepek, T. Vrtač, G. Čepon, M. Boltežar
University of Ljubljana, Faculty of Mechanical Engineering,
Aškerčeva 6, 1000 Ljubljana

Abstract
In noise and vibration engineering, a structure's passive dynamic properties are often evaluated in terms of its frequency response functions (FRFs). The typical FRF measurement campaign consists of controlled structure excitation and the capturing of its response. However, exploiting operational excitation for FRF acquisition is not feasible, with many sources simply too complex to model or measure directly. In the present paper, an alternative approach is proposed for an indirect FRF estimation of a system in operation, in which the source is characterized independently of the final assembly. To overcome the issue of the unmeasurable excitation force, transfer path analysis (TPA) methods are proposed. TPA replicates the source excitations using the set of equivalent or pseudo forces that are an inherent property of the source. The assembly's FRFs are then evaluated on the basis of receiver responses and pre-determined pseudo forces for independent operational load cases at the source. Thus, a single source description can be applied to estimate the FRFs of any assembly with an identical source and arbitrary passive side.

1 Introduction

The dynamic properties of assembled products are commonly determined using an experimental approach through the measurement of FRFs. This is typically carried out on a non-operating system, where the structure is excited using an impact hammer or shaker while capturing the response. Although it is common that assembly products are excited by inner sources while they are operating, using operational excitation for a FRF measurement is not feasible, as many of the sources are too complex to model or measure.

The ability to obtain a system's FRFs while it is operating was proposed by de Klerk and Valentin [1]. Operational system identification (OSI) utilizes a superposition method to eliminate the contribution of the unmeasurable operational forces and retains only the shaker's excitation force. This also takes into account the influence of different operating states on the dynamic properties of the system.

On the other hand, sources that are impossible to measure can be characterized using a TPA. For this, a set of forces, applied at the interfaces between the source and the receiver structure, is estimated. These forces replicate the responses at the receiver, initially generated by the vibrating source. Two conceptually different families of TPA methods can be applied accordingly: classical and component-based TPA [2]. Classical TPA methods describe source excitations using the interface forces [3]. This approach has one major drawback, as the determined forces are only valid for the measured assembly. For an independent characterization of the source, a component-based TPA adopts a different approach. Here, a set of equivalent forces counteracts the operational excitation and thus blocks the motion downstream of the interface. These equivalent or blocked forces are valid for any assembly with a modified receiver [2, 4].

The load on the interface for the TPA can be measured directly or indirectly. A direct load determination using force transducers mounted at the interface is difficult in practice [5]. The indirect determination of the forces at the interface in multiple degrees of freedom (DoFs) using an inverse procedure is, therefore, often preferable. Different admittance-based TPA methods for the various boundary conditions of the active component were proposed over the years [2], with the in-situ TPA [6] even eliminating the need to dismount

any part of the assembly. Similar advantages are offered by the pseudo-force-based TPA, where the source is characterised using a set of pseudo forces. The method was first proposed by Janssens and Verheij [7] and has gained popularity since [5, 8].

The concept of using source characterization for an indirect FRF estimation has already been proposed by numerous authors and demonstrated by several successful implementations. By using directly measured interface loads and responses on the assembly, passive substructure FRFs can be obtained [9], related to a classical TPA. Using equivalent forces as a source descriptor, a round-trip identity method has been proposed [10, 11] and recently extended [12]. The method allows for indirect FRF measurements at locations that are otherwise hindered by inaccessibility, uncontrollability of the force input or a poor signal-to-noise ratio. In [13], pseudo-force-based TPA was employed to indirectly obtain assembly FRFs using operational excitation. However, an important aspect of equivalent forces, i.e., their transferability to modified assemblies, has not yet been explored for FRF estimations.

In this work an independent source characterization is exploited to estimate the FRFs of the product assembly. The approach is based on the assembly being divided into two substructures: the active and the passive side. On the active side, the source excitation is present while the assembly is subjected to operational conditions. Meanwhile, no excitation force is active on the passive side. Using component-based TPA methods, source excitations are expressed in terms of the pseudo forces (or equivalent forces from any other component-based TPA approach). These forces are only a property of the source and are thus transferable to an assembly with the modified passive side. Given that the pseudo forces are known, assembly FRFs can be evaluated based only on a receiver-response measurement, carried out on the assembly while it is operating. This is also valid and especially convenient for cases when the passive side is modified. Measurements are repeated several times for independent load cases to allow for inverse system identification [14]. The FRFs of the modified assembly are then estimated with no additional excitation measurements required on the novel assembly.

2 FRF estimation using source characterization

2.1 Pseudo-force-based TPA

Consider a linear and time-invariant assembly of substructures A and B, coupled at the interface, as depicted in Fig. 1a. Substructure A is an active component with operational excitation $\boldsymbol{f}_1$ acting on internal source DoFs. Meanwhile, no excitation force is present on the passive substructure B. The responses on B are hence a consequence of $\boldsymbol{f}_1$ only, and are observed in three different sets of DoFs: at the interface DoFs ($\boldsymbol{u}_2$), in the proximity of the interface at the indicator DoFs ($\boldsymbol{u}_4$), and away from the interface at the target DoFs ($\boldsymbol{u}_3$).

In practice, most of the sources generate an input force $\boldsymbol{f}_1$ that is impossible to measure. A quantity that, by itself, allows a full description of the source for a given operational condition is therefore required. A set of pseudo forces $\boldsymbol{f}_{\mathrm{ps}}$, located at the internal source DoFs, is introduced that generates the same operational responses at the indicator DoFs as $\boldsymbol{f}_1$[1]:

$$\boldsymbol{u}_4 = \mathbf{Y}_{41}^{\mathrm{AB}} \boldsymbol{f}_1 = \mathbf{Y}_{4\mathrm{ps}}^{\mathrm{AB}} \boldsymbol{f}_{\mathrm{ps}}, \tag{1}$$

where $\mathbf{Y}_{4\mathrm{ps}}^{\mathrm{AB}}$ is a transfer-path admittance, relating the motion at the indicator DoFs to the pseudo forces. Expressing $\boldsymbol{f}_{\mathrm{ps}}$ from the indicator responses $\boldsymbol{u}_4$ yields:

$$\boldsymbol{f}_{\mathrm{ps}} = \left(\mathbf{Y}_{4\mathrm{ps}}^{\mathrm{AB}}\right)^{+} \boldsymbol{u}_4, \tag{2}$$

where $(\star)^{+}$ denotes a pseudo inverse[2]. The application of both operational forces $\boldsymbol{f}_1$ and the pseudo forces

[1] An explicit dependency on the frequency is omitted to improve the readability of the notation, as will be the case for the remainder of the paper.

[2] It is common practice to overdetermine the system by adding additional responses at the indicator DoFs. This ensures the interface is properly observable from $\boldsymbol{u}_4$.

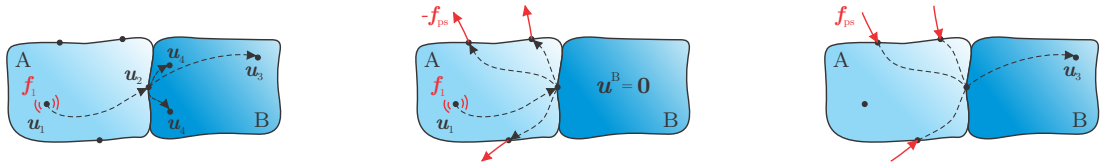

(a) (b) (c)

Figure 1: Pseudo-force-based TPA; a) assembly of substructures A and B, b) pseudo forces blocking the motion at the interface, c) pseudo forces generating same responses $\boldsymbol{u}_3$ as $\boldsymbol{f}_1$.

$\boldsymbol{f}_{\mathrm{ps}}$ acting in the opposite direction annuls any response on the passive side (Fig. 1b):

$$\mathbf{0} = \mathbf{Y}_{41}^{\mathrm{AB}} \boldsymbol{f}_1 + \mathbf{Y}_{4\mathrm{ps}}^{\mathrm{AB}} \big(- \boldsymbol{f}_{\mathrm{ps}} \big). \tag{3}$$

Two conclusions can be drawn from this: the pseudo forces are a valid source description for any passive side. Therefore, they are transferable to an assembly with a modified receiver. Secondly, operational responses on the receiver can be replicated by the set of pseudo forces (Fig. 1c) as:

$$\boldsymbol{u}_3 = \mathbf{Y}_{3\mathrm{ps}}^{\mathrm{AB}} \boldsymbol{f}_{\mathrm{ps}}. \tag{4}$$

Given that the interface behaves rigidly, six (s = 6) pseudo forces are considered sufficient for a valid source characterization. This number should be increased for a more intricate connectivity. Although the positions of the pseudo forces on active side are arbitrary, care should be taken to select impact excitations that ensure full controllability of the interface modes, thus making these forces independent of the receiver.

2.2 FRF estimation from the pseudo forces

Having introduced the concept of pseudo forces describing unmeasurable excitations, a new approach to an indirect FRF estimation on operational assemblies is proposed in the following. The approach consists of two stages: independent source characterization on the original assembly, denoted by AB (e.g., dedicated laboratory test-bench), and an operational response measurement on the final assembly $\mathrm{A}\widetilde{\mathrm{B}}$.

Let us assume that the operational excitation is able to generate enough mutually independent load cases $\mathbf{F}_1 = \left[\boldsymbol{f}_1^{(1)}, \ldots, \boldsymbol{f}_1^{(i)}, \ldots, \boldsymbol{f}_1^{(m)} \right]$, where $i \in \{1, \ldots, m\}$ (e.g., during engine run-up). For m independent

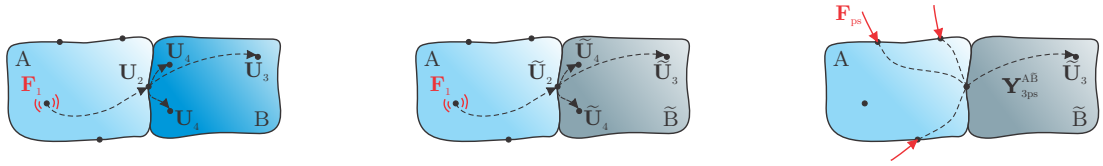

(a) (b) (c)

Figure 2: FRF estimation from pseudo forces; a) initial assembly subjected to independent load cases, a) modified assembly in operation, c) FRF estimation on modified assembly.

load cases at the source (Fig. 2a), m sets of pseudo forces can be estimated from measurements made on AB using Eq. (2). The corresponding vectors $\boldsymbol{f}_{\mathrm{ps}}^{(i)}$ can be stored as columns in[3]:

$$\mathbf{F}_{\mathrm{ps}} = \left[\boldsymbol{f}_{\mathrm{ps}}^{(1)}, \ldots, \boldsymbol{f}_{\mathrm{ps}}^{(i)}, \ldots, \boldsymbol{f}_{\mathrm{ps}}^{(m)} \right] \in \mathbb{C}^{s \times m}. \tag{5}$$

[3]Any other component-based TPA approach can be applied at this stage to estimate the forces, equivalent to the operational excitation and assemble the force matrix $\mathbf{F}$.

As the pseudo forces are only a property of the source, the same active side can then be attached to any novel receiver (Fig. 2b), thus forming a modified assembly $\mathrm{A}\widetilde{\mathrm{B}}$. There, the set of m responses from the exact same m load cases $\boldsymbol{f}_1$ is obtained at the n_3 target DoFs, denoted by $\widetilde{\boldsymbol{u}}_3$:

$$\widetilde{\mathbf{U}}_3 = \left[\widetilde{\boldsymbol{u}}_3^{(1)}, \ldots, \widetilde{\boldsymbol{u}}_3^{(i)}, \ldots, \widetilde{\boldsymbol{u}}_3^{(m)}\right] \in \mathbb{C}^{n_3 \times m}. \tag{6}$$

Provided that m is equal to or larger than s and the inverse of $\mathbf{F}_{\mathrm{ps}}$ exists, the admittance matrix $\mathbf{Y}_{3\mathrm{ps}}^{\mathrm{A}\widetilde{\mathrm{B}}}$ of the novel assembly (Fig. 2c) can be estimated:

$$\left[\widetilde{\boldsymbol{u}}_3^{(1)}, \ldots, \widetilde{\boldsymbol{u}}_3^{(i)}, \ldots, \widetilde{\boldsymbol{u}}_3^{(m)}\right] = \mathbf{Y}_{3\mathrm{ps}}^{\mathrm{A}\widetilde{\mathrm{B}}} \left[\boldsymbol{f}_{\mathrm{ps}}^{(1)}, \ldots, \boldsymbol{f}_{\mathrm{ps}}^{(i)}, \ldots, \boldsymbol{f}_{\mathrm{ps}}^{(m)}\right], \tag{7}$$

$$\mathbf{Y}_{3\mathrm{ps}}^{\mathrm{A}\widetilde{\mathrm{B}}} = \widetilde{\mathbf{U}}_3 \, \mathbf{F}_{\mathrm{ps}}^{+}. \tag{8}$$

This is referred to as an inverse system identification. $\mathbf{Y}_{3\mathrm{ps}}^{\mathrm{A}\widetilde{\mathrm{B}}}$ is a FRF matrix, relating the motion at the target DoFs to pseudo forces. As seen from Eq. (8), a single source description can be applied to estimate the FRFs of any assembly with the modified passive side. Note that this approach relies on the case with source excitation acting solely on the active and responses $\widetilde{\boldsymbol{u}}_3$ acquired only on the passive side of the assembly.

If we expand Eq. (8):

$$\mathbf{Y}_{3\mathrm{ps}}^{\mathrm{A}\widetilde{\mathrm{B}}} = \widetilde{\mathbf{U}}_3 \left[\left(\mathbf{Y}_{4\mathrm{ps}}^{\mathrm{AB}}\right)^{+} \boldsymbol{u}_4^{(1)}, \ldots, \left(\mathbf{Y}_{4\mathrm{ps}}^{\mathrm{AB}}\right)^{+} \boldsymbol{u}_4^{(i)}, \ldots, \left(\mathbf{Y}_{4\mathrm{ps}}^{\mathrm{AB}}\right)^{+} \boldsymbol{u}_4^{(m)}\right]^{+} = \widetilde{\mathbf{U}}_3 \left(\left(\mathbf{Y}_{4\mathrm{ps}}^{\mathrm{AB}}\right)^{+} \mathbf{U}_4\right)^{+}, \tag{9}$$

two observations can be made. Firstly, the experimental effort for the indirect FRF estimation on $\mathrm{A}\widetilde{\mathrm{B}}$ comprises $\mathbf{Y}_{4\mathrm{ps}}^{\mathrm{AB}}$ and $\mathbf{U}_4$ measurements performed on AB, and the $\widetilde{\mathbf{U}}_3$ measurement conducted on $\mathrm{A}\widetilde{\mathrm{B}}$. Secondly, we observe that two inversions occur in the process, which are addressed in the following.

2.3 Inverse problem

As is usually the case with inverse methods, Eq. (8) might be ill-conditioned[4]. Given that the condition number of the matrix to be inverted is high, this can lead to a major amplification of the error in the results. To address this issue, regularization techniques are proposed, such as singular-value truncation or Tikhonov regularization [15].

Let us first look at a special case when the number of pseudo forces is equal to the number of indicator responses ($s = n_4$) and therefore $\mathbf{Y}_{4\mathrm{ps}}^{\mathrm{AB}} \left(\mathbf{Y}_{4\mathrm{ps}}^{\mathrm{AB}}\right)^{+} = \mathbf{I}$. Assuming that operational excitations are mutually independent, so that $\mathbf{U}_4 \left(\mathbf{U}_4\right)^{+} = \mathbf{I}$, the inverse of the pseudo force matrix for such cases can be simplified to:

$$\mathbf{F}_{\mathrm{ps}}^{+} = \left(\mathbf{U}_4\right)^{+} \mathbf{Y}_{4\mathrm{ps}}^{\mathrm{AB}}. \tag{10}$$

Consequently, Eq. (8) becomes:

$$\mathbf{Y}_{3\mathrm{ps}}^{\mathrm{A}\widetilde{\mathrm{B}}} = \widetilde{\mathbf{U}}_3 \left(\mathbf{U}_4\right)^{+} \mathbf{Y}_{4\mathrm{ps}}^{\mathrm{AB}}. \tag{11}$$

Hence, for this special case the regularization only applies to the $\mathbf{U}_4$ matrix.

This does not directly apply if the Eq. (2) is overdetermined, as $n_4 > s$ and consequently $\mathbf{Y}_{4\mathrm{ps}}^{\mathrm{AB}} \left(\mathbf{Y}_{4\mathrm{ps}}^{\mathrm{AB}}\right)^{+} \neq \mathbf{I}$. Nevertheless, similar reasoning can be used to regularize $\mathbf{U}_4$ in Eq. (9) only.

3 Numerical study

The following section demonstrates the proposed approach for the FRF estimation. To clearly present the idea, the method is first depicted on a synthetic, numerical case study.

[4]For the numerical models this should not pose a problem as each interface mode will have some (although small) contribution at each frequency point.

3.1 Numerical model

The numerical benchmark, presented in Fig. 3, consists of two substructures, referred to as active side A (source) and passive side B (receiver). Both are beam-like aluminium structures and are perfectly bonded at the interface. They are selected to display a number of well-separated flexible vibration modes within the frequency range of interest, i.e., 0–2000 Hz. The assembly is subjected to free boundary conditions.

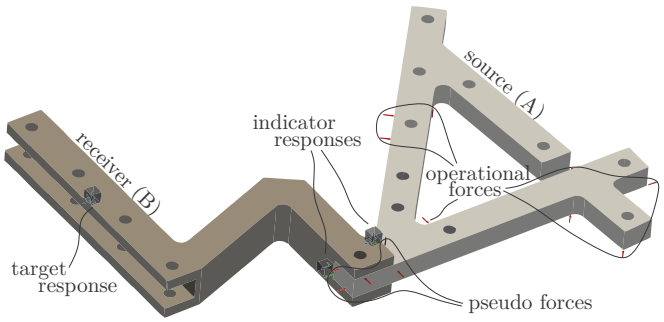

Figure 3: Numerical model.

Due to the use of a single-point connection type, where the relatively small contact area ensures the connectivity between the substructures, an assumption of rigid interface behaviour is adopted in the following. Six (s = 6) positions of the pseudo forces were chosen close to the interface on the active side. These impact positions were equally distributed over the interface and between all the directions to maximize the interface controllability. Nine response locations were selected in the vicinity of the interface on the passive side (indicator DoFs) and three away from the interface (target DoFs). The transfer-path admittances $\mathbf{Y}_{4\mathrm{ps}}^{\mathrm{AB}}$ and $\mathbf{Y}_{3\mathrm{ps}}^{\mathrm{AB}}$ were calculated using the Python package *pyFBS* [16]. Away from the interface on the active side, 12 locations were defined, where operational excitation was applied.

3.2 Source characterization

The internal operating forces were simulated by applying linear sine-sweep signals (length 10 s, frequency range from 0.1 Hz to 2000 Hz) with different amplitudes and phase relations at 12 predefined force locations. The total response was then divided into m = 10 individual time blocks, each with a length of 1 s. The pseudo forces were computed for each of these time blocks individually using Eq. (2). An evaluation of the pseudo forces' consistency can be performed in terms of on-board validation, using the responses to the load cases at the channels away from the interface [17, 18]. These responses can be predicted directly from the pseudo forces (Eq. (4)). Comparing the measured and predicted response serves as the initial check for the source description's completeness[5]. An on-board validation for the first time block at the selected channel is shown in Fig. 4a. The correlation between the two responses is additionally evaluated using the coherence criterion [18]:

$$\mathrm{coh}(x,\, y) = \frac{(x+y)(x^*+y^*)}{2(x^*x+y^*y)} \quad x \in \boldsymbol{u}_3^{\mathrm{p}},\, y \in \boldsymbol{u}_3^{\mathrm{m}}, \tag{12}$$

where $(\star)^*$ denotes a complex conjugate, while the superscripts $(\star)^{\mathrm{p}}$ and $(\star)^{\mathrm{m}}$ refer to the predicted and measured target responses, respectively. The frequency-dependent criterion is evaluated for the entire frequency range and then averaged[6]. The mean coherence values from all the target DoFs are presented in Fig. 4b for individual time blocks. Coherence values are found to be high for all the time blocks; hence, it can be concluded that pseudo forces describe the operational excitation sufficiently well.

[5]Poor agreement between the measured and predicted responses indicates that there might be other, unobserved and uncontrolled, transfer paths that contribute to the target output.

[6]The criterion is bounded between 0 and 1, with values closer to 1 indicating a strong correlation between the compared responses.

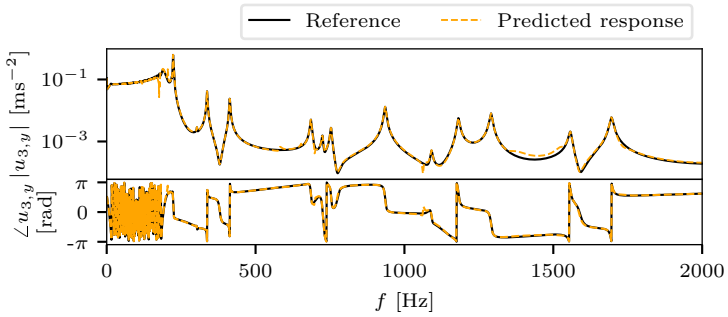

(a)

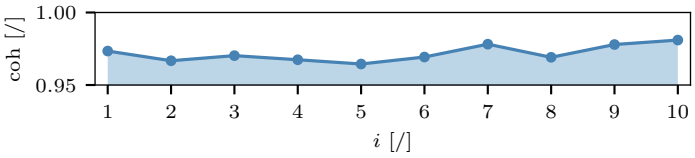

(b)

Figure 4: On-board validation; a) predicted and reference responses $u_{3,y}$ for the first time block, b) coherence between predicted and reference responses for all target DoFs and all individual time blocks.

3.3 Interface as bottleneck

This section briefly addresses the observability and controllability of the interface, which must be taken into account to properly describe the source excitations and estimate the assembly FRFs. The remarks are developed based on the findings presented in [5]. In the following we assume m independent load cases, so that the rank of $\mathbf{F}_1$ is equal to m. These load cases excite the interface modes, which are observed from n_4 indicator DoFs on the passive side. However, the number of independent interface modes seen from $\boldsymbol{u}_4$ can only be equal to or less than the interface DoFs n_2 (rank$(\mathbf{U}_4) \leq n_2$), although it is recommended that $n_4 > n_2$. This is referred to as the bottleneck effect (Fig. 5). To ensure full interface observability and controllability, n_2 interface modes should be excited by m load cases ($m \geq s$) and observed by n_4 indicator DoFs. These conditions are independent of the number of target DoFs.

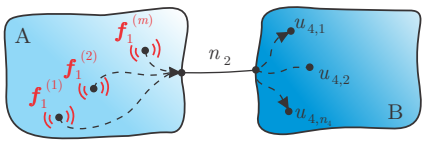

Figure 5: Interface acting as bottleneck with n_2 DoFs.

Due to the assumption of rigid interface behaviour, a number of $n_2 = 6$ interface modes should be observed from the indicator DoFs, meaning that the rank of $\mathbf{U}_4$ is equal to n_2. This also means all six interface modes are properly excited from the applied load cases. A quick assessment indicating the number of excited and observed interface modes can be found in the form of a singular value decomposition (SVD) tool. When applied to the $\mathbf{U}_4$ matrix:

$$\mathbf{U}_4 = \mathbf{U}\,\mathbf{\Sigma}\,\mathbf{V}^{\mathrm{H}}, \tag{13}$$

the columns of $\mathbf{U}$ and $\mathbf{V}$ are the left- and right-hand singular vectors of $\mathbf{U}_4$, while $\mathbf{\Sigma}$ is a diagonal matrix containing singular values of $\mathbf{U}_4$[7]. Fig. 6a shows the singular values of the $\mathbf{U}_4$ matrix. It is clear that six significant singular values are observed. This is further verified in Fig. 6b, where the ratio between the sum of the first six against the sum of all the singular values is depicted. The ratio approaches one across the

[7]The superscript $(\star)^{\mathrm{H}}$ denotes the Hermitian (complex conjugate transpose) operator.

entire frequency range of interest, indicating six independent modes being observed from $\boldsymbol{u}_4$. The interface is fully controllable and fully observable, thus $s = 6$ pseudo forces are sufficient to excite the interface modes and represent the source independently of the passive side.

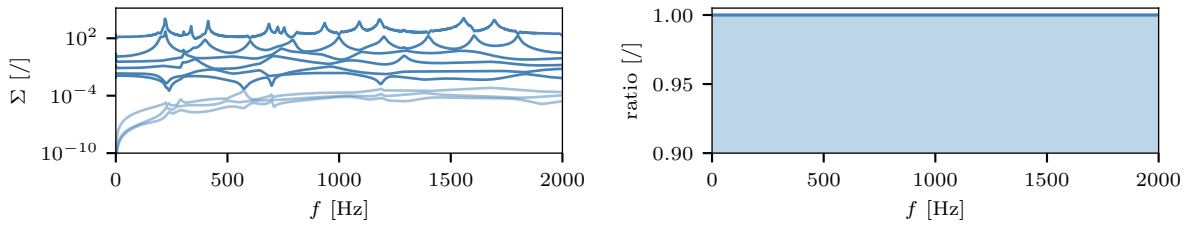

(a) (b)

Figure 6: Interface observability and controllability; a) singular values of $\mathbf{U}_4$, b) ratio between sum of the first six against sum of all singular values.

Although Fig. 6 shows six significant singular values, this may not necessarily indicate that the interface has six DoFs. It might be that the operational load cases are not able to excite more than six independent interface modes. It is good practice to apply additional load cases and observe the changes in the singular values of $\mathbf{U}_4$, such that $m > n_4$ [5]. Given that the number of significant singular values increases, placing additional pseudo forces at the source should be considered.

3.4 FRF estimation for the initial assembly

An estimation of the assembly's FRFs is first carried out on a non-modified structure from Fig. 3. Pseudo forces from all m load cases are stacked in the $\mathbf{F}_{\text{ps}}$ matrix (Eq. (5)). Operational responses $\boldsymbol{u}_3$ to the same m load cases are stored in $\mathbf{U}_3$ (Eq. (6)). FRFs relating to the responses at the three channels away from the interface to pseudo forces ($\mathbf{Y}^{\text{AB}}_{\text{3ps}}$) are then calculated using Eq. (8). An example of the FRF for one pseudo force and one response location is shown in Fig. 7, compared to the true reference FRF. Minor discrepancies are found in the same frequency bands where on-board validation shows a deficient source characterization; however, good overall agreement between the FRFs can be observed.

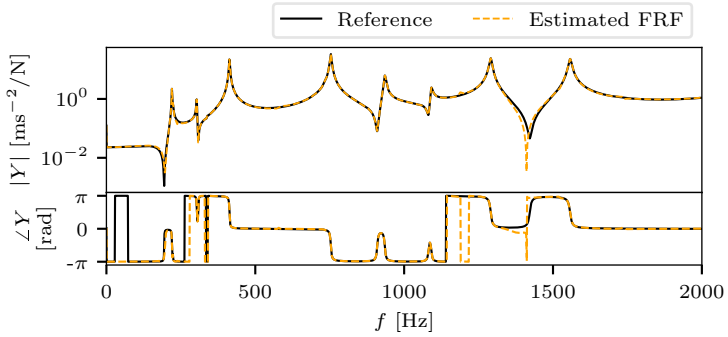

Figure 7: FRF of the initial assembly for excitation $f_{\text{ps},6}$ and response $u_{3,x}$ obtained from an independent source characterization.

To objectively evaluate the consistency of the estimated FRFs, a coherence criterion (Eq. (12)) is adopted. Fig. 8 shows the averaged coherence between the estimated FRFs and the reference for all channels and all pseudo-force excitations. High coherence values can be observed for all FRFs, indicating the high consistency of the estimated FRFs.

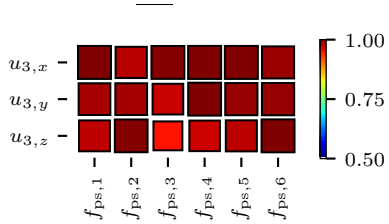

Figure 8: Frequency-averaged value of the coherence criterion between the estimated and reference FRFs for the initial assembly.

3.5 FRF estimation on modified assembly

As depicted in Fig. 9, an additional beam-like structure was then mounted on the original substructure B, thus modifying the receiver side of the assembly. Using the same m load cases at the same 12 excitation locations on the active side, the responses $\widetilde{\boldsymbol{u}}_3$ at the receiver were simulated. In such a manner, source excitations are independent of the receiver.

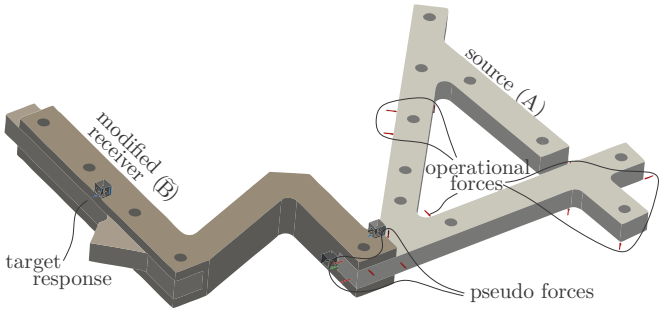

Figure 9: Modified numerical model.

The target responses to different load cases $\widetilde{\boldsymbol{u}}_3^{(i)}$ are stacked as columns in the matrix $\widetilde{\mathbf{U}}_3$ (Eq. (6)). Using pseudo forces identified on the non-modified assembly ($\mathbf{F}_{\mathrm{ps}}$), the FRFs of the modified assembly are estimated using Eq. (8). Fig. 10 shows good agreement between the estimated and reference FRFs. Again, small drops in FRF consistency are observed in regions where the source is imperfectly characterized. The correct global dynamic parameters (e.g., natural frequencies) of the novel assembly can be identified from the estimated FRFs, without the need for additional characterization of the excitation force .

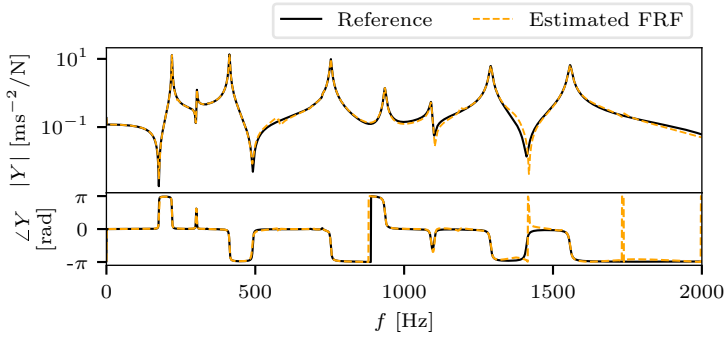

Figure 10: FRFs of the modified assembly for excitation $f_{\mathrm{ps},6}$ and response $\widetilde{u}_{3,y}$ obtained from an independent source characterization.

Using the coherence criterion, a high consistency for the estimated FRFs on a novel assembly is again observed (Fig. 11).

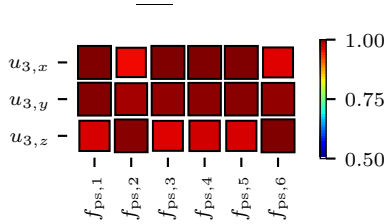

Figure 11: Frequency-averaged value of the coherence criterion between the estimated and reference FRFs on the modified assembly.

4 Experiment

4.1 Experimental setup

To demonstrate the applicability of the proposed approach, an experimental case study is presented next. An assembly of two aluminium beam-like substructures is presented in Fig. 12a. Structure A is considered as active and B as a passive side. The connectivity at the interface of the assembly is ensured by an M10 bolt with a locking nut, top/bottom washers and a tightening torque of approximately 20 Nm. The same connection type is used to attach the passive side to the approximately fixed ground. Due to using a single-point connection type, the assumption of rigid interface behaviour is adopted in the following.

Three triaxial modal accelerometers PCB 356A32 were fixed close to the interface on the passive side (measuring the indicator DoFs' response $\boldsymbol{u}_4$) as depicted in Fig. 12b. An additional accelerometer of the same type was mounted on the receiver, but away from the interface (measuring the target response $\boldsymbol{u}_3$, Fig. 12a). Close to the interface on the active side, six triangular blocks milled from solid aluminium were glued to the surface using cyanoacrylate glue (Fig. 12b). These served as the position for the pseudo forces, making it possible to excite all the interface modes and ensure full interface controllability. The excitations were performed using the PCB 086C03 modal hammer with a vinyl tip. The transfer-path admittance ($\mathbf{Y}_{4\mathrm{ps}}^{\mathrm{AB}}$ and $\mathbf{Y}_{3\mathrm{ps}}^{\mathrm{AB}}$) was then measured, with eight impact repetitions per individual pseudo-force location.

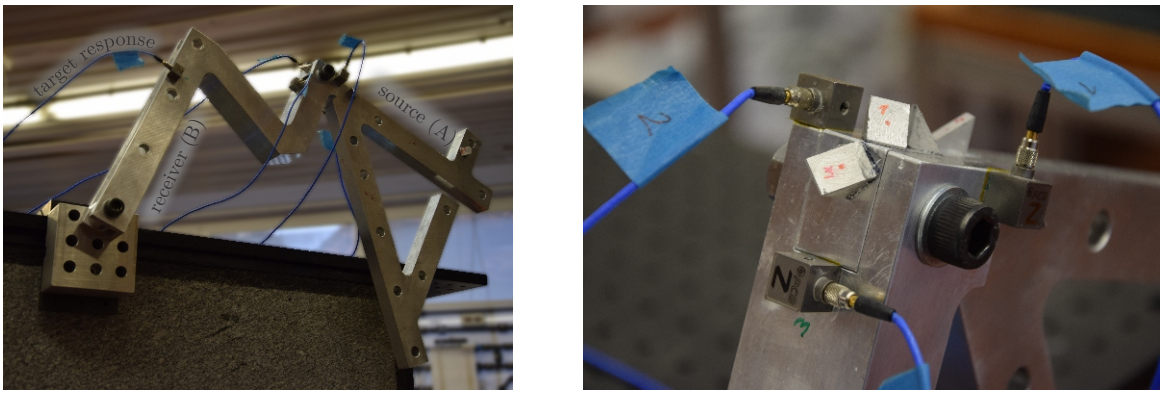

(a) (b)

Figure 12: Experimental setup; a) beam-like structure, b) positions of $\boldsymbol{f}_{\mathrm{ps}}$ and $\boldsymbol{u}_4$.

For the operational excitations, 12 impact locations were arbitrarily selected on the active side away from the interface. Each location was individually excited, hence 12 independent load cases were introduced, while the responses on the passive side were captured. No impact repetitions were performed for the operational excitations, thus accounting for the random errors that were present (e.g., measurement noise, random errors in impact location and orientation) while operating.

4.2 FRF estimation on the initial assembly

First, the interface observability and controllability are analysed. Fig. 13a shows singular values of the measured $\mathbf{U}_4$. The ratio between the sum of the first six against the sum of all the singular values is presented in Fig. 13b.

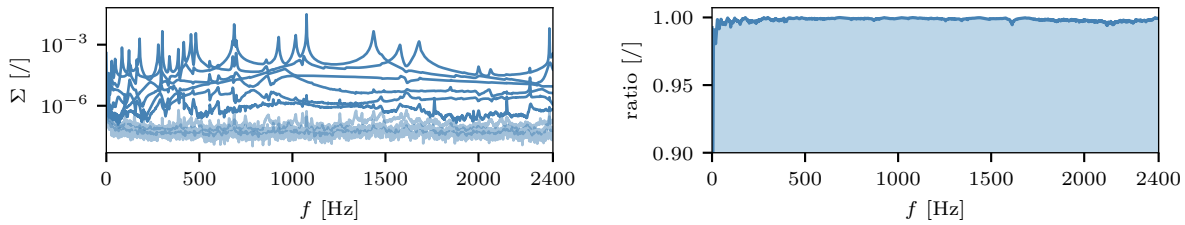

(a) (b)

Figure 13: Interface observability and controllability of the experimental example; a) singular values of $\mathbf{U}_4$, b) ratio between sum of the first six against sum of all singular values.

Only a slight drop of the ratio is observed in the very-low-frequency range, which is a consequence of the poor signal-to-noise ratio as the structure behaves rather rigidly at these frequencies. Six interface modes, excited by independent load cases, are therefore observable from the indicator DoFs. This also justifies the assumption of interface rigidity.

The FRFs are first evaluated on the initial assembly, following the same procedure that was explained in more detail in Section 3. For each load case, the vector of pseudo forces $\boldsymbol{f}_{\mathrm{ps}}$ is estimated. The passive side responses $\boldsymbol{u}_3$ are simultaneously obtained for the same load cases. Both respective quantities are stacked in the $\mathbf{F}_{\mathrm{ps}}$ and $\mathbf{U}_3$ matrices. Using an inverse system identification (Eq. (8)), the assembly FRFs $\mathbf{Y}_{3\mathrm{ps}}^{\mathrm{AB}}$ are obtained. Fig. 14 shows an example of the estimated FRF against the reference. Across the entire frequency range, good agreement is observed between the two. Only slight differences are present in the frequency regions where the response magnitude is low, contributing to the poor signal-to-noise ratio. The high FRF consistency is additionally confirmed by the coherence criterion for all the evaluated DoFs (Fig. 15).

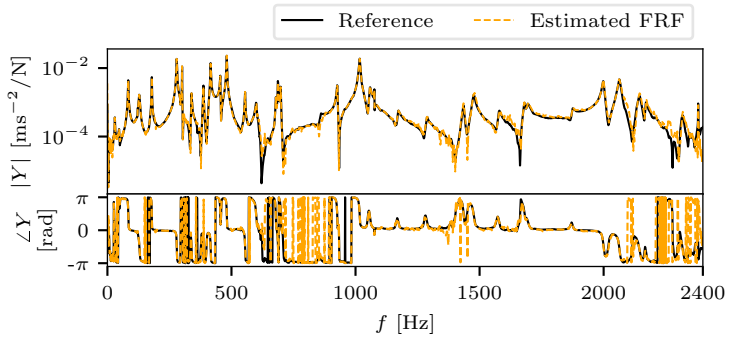

Figure 14: FRFs of the initial assembly for excitation $f_{\mathrm{ps},6}$ and response $\widetilde{u}_{3,x}$ obtained from an independent source characterization.

4.3 FRF estimation on modified assembly

After the FRF estimation of the initial assembly, the latter was modified with the new passive side introduced. As depicted in Fig. 16, an additional beam-like structure was bolted to the original substructure B, again using M10 bolts and a tightening torque of 20 Nm. To obtain the responses of the modified assembly to the same load cases as for the initial assembly, first the FRFs between the load-case locations and the target-response

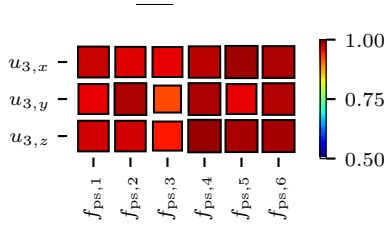

Figure 15: Frequency-averaged value of the coherence criterion between the investigated and reference FRFs on the initial assembly.

channels were measured, again using only one impact repetition per load case. FRFs were then multiplied by the measured force from the initial assembly, hence imitating the same independent load cases. In this manner, operational responses $\widetilde{\boldsymbol{u}}_3$ were obtained.

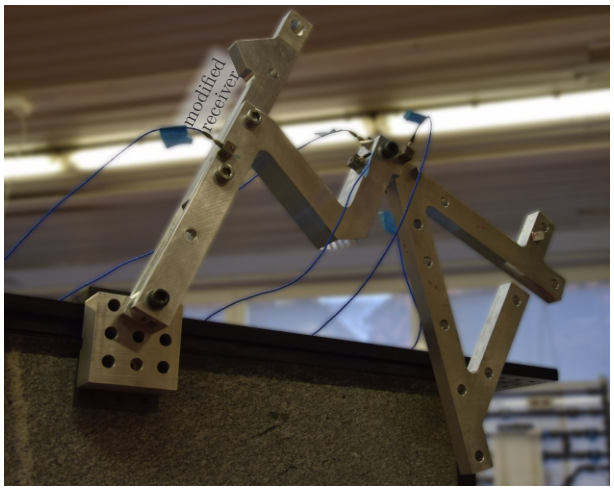

Figure 16: Modified beam-like structure.

From $\widetilde{\boldsymbol{u}}_3$ responses, the $\widetilde{\mathbf{U}}_3$ matrix was built. Tikhonov regularization was used in this experimental example to regularize the matrix $\mathbf{U}_4$ when calculating novel assembly FRFs $\mathbf{Y}_{3\mathrm{ps}}^{\mathrm{A}\widetilde{\mathrm{B}}}$. The regularization parameter α was determined using the Wiener filter [19] where the noise was recorded for the case when no load was applied. By comparing estimated FRF to the reference (Fig. 17), it is clear that a consistent frequency response can be obtained for the modified assemblies using independent source characterization, especially in the low-frequency range. In the high-frequency range, the overall consistency of the estimated FRFs is still high, but shows some discrepancies, presumably due to minor inconsistencies in the load cases applied (impact location and orientation errors compared to the load cases on the initial assembly).

The coherence criterion was then used to evaluate the overall agreement between the regularized FRFs and the reference. The results are presented in Fig. 18 and indicate high consistency of indirectly determined FRFs.

5 Application study

In the following, a method's applicability to real complex structures is demonstrated. A source structure is a brushless permanent-magnet (BPM) motor, which is first mounted on a dedicated test-bench, presented in Fig. 19a. The connectivity between the BPM motor and the receiver side of the assembly is ensured by four mounting points using M8 threaded rods with a tightening torque of 5 Nm. At the source, 12 pseudo force locations (3 per mounting point) were defined, all located in the proximity of the mounting and evenly

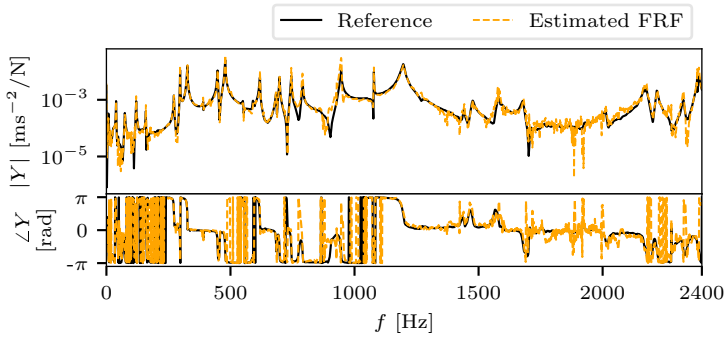

Figure 17: FRFs of the modified assembly for excitation $f_{\mathrm{ps},6}$ and response $\widetilde{u}_{3,x}$ obtained from an independent source characterization.

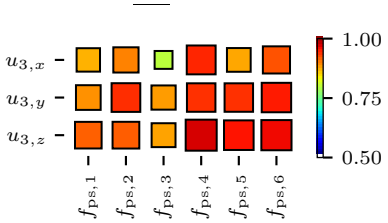

Figure 18: Frequency-averaged value of the coherence criterion between the estimated and reference FRFs on the modified assembly.

distributed in all directions. 8 triaxial accelerometers (2 per mounting point) were positioned at the indicator DoFs of the test-bench, with an additional accelerometer added to measure target responses. Transfer-path admittance $\mathbf{Y}^{\mathrm{AB}}_{4\mathrm{ps}}$ was obtained for the frequency range of interest (0–1000 Hz) by impact testing.

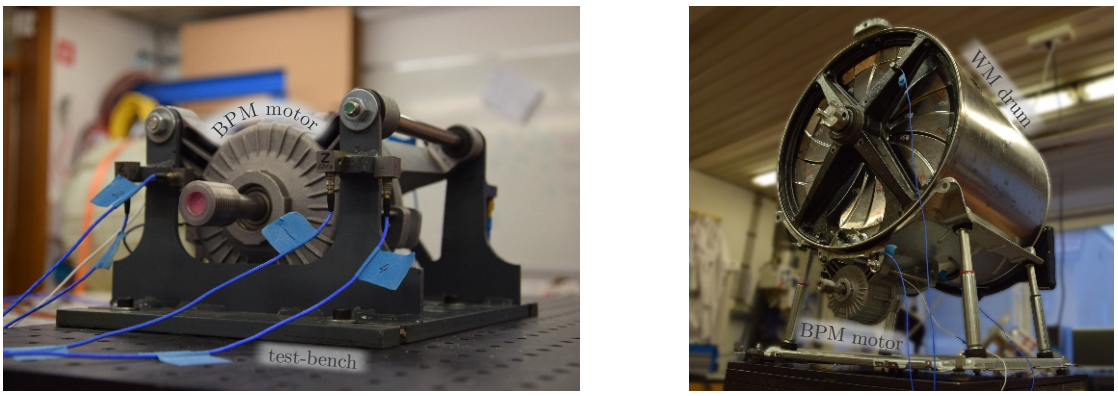

(a) (b)

Figure 19: Experimental setup; a) a BPM motor on a test-bench, b) washing machine (WM) drum assembly.

Operational excitation consisted of a BPM motor run-up from 0 Hz to 336 Hz with an angular acceleration of 9.3 $\frac{\mathrm{Hz}}{\mathrm{s}}$. In total, 36 s of response was captured and cropped into 1 s long individual time blocks without overlapping. Individual responses at the target and indicator DoFs were stacked into $\mathbf{U}_3$ and $\mathbf{U}_4$ matrices, respectively. A BPM motor was then mounted on the washing machine drum (Fig. 19b) where three triaxial accelerometers were used to capture the target response. The same excitation regime as for the test-bench setup was run on a washing machine drum, thus obtaining matrix $\widetilde{\mathbf{U}}_3$.

An inspection of excitations' mutual independency was performed first. For this, matrix $\mathbf{U}_4$ was used. By

evaluating $\mathbf{U}_4 \left(\mathbf{U}_4\right)^+$, identity matrix $\mathbf{I}$ should be obtained at each frequency point. Results are presented in Fig. 20, where $\mathbf{U}_4 \left(\mathbf{U}_4\right)^+$ is summed over all frequency points, thus comprising the examination for the entire frequency range of interest. It is evident that BPM motor run-up is able to generate sufficient number of independent load cases for the inverse system identification.

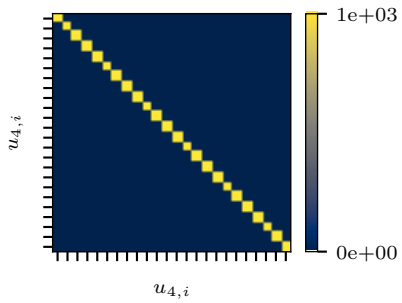

Figure 20: Sum of $\mathbf{U}_4 \left(\mathbf{U}_4\right)^+$ over all frequency points.

Again, FRFs were estimated for both the initial and modified assemblies, using Eq. 9. Tikhonov regularization was applied to regularize $\mathbf{U}_4$. Fig. 21 shows an example of estimated FRF on an assembly of a BPM motor and a test-bench. Compared to the reference, good agreement is observed, with the exception of the low frequency range (0–150 Hz). This is believed to be due to the stiff nature of the test-bench and consequently poor SNR at low frequencies. An additional drawback of the experimental setup is the low amplitude of the responses during the operation of the BPM motor, reaching up to a maximum of 30 $\frac{\mathrm{m}}{\mathrm{s}^2}$ only over the full time series. Hence discrepancies can be found at estimated anti-resonance regions throughout the entire frequency range of interest.

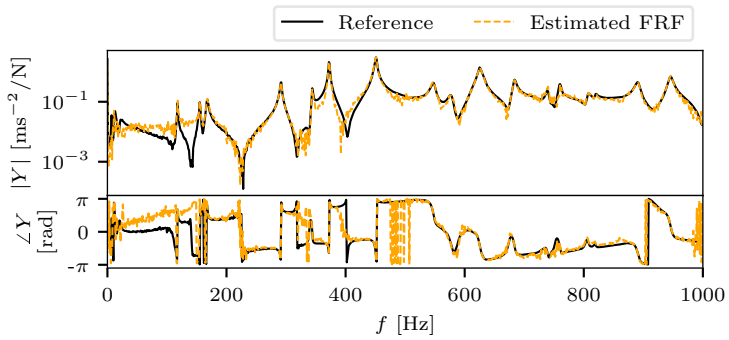

Figure 21: FRFs of a BPM motor and a test-bench assembly for excitation $f_{\mathrm{ps},1}$ and response $u_{3,3}$.

Indirectly obtained FRF for the washing machine drum assembly shows an amplitude-wise meaningful estimation, when compared to the reference (Fig. 22). Differences are apparent throughout the entire examined frequency range due to the high modal density of the washing machine drum. Sources of errors can be found in local non-linearities introduced by components such as vibro-isolations or suspension elements, and in imperfect repeatability of the excitation regime. Due to the two above-stated reasons, related to the complexity of the structure used for this study, pseudo forces have limited transferability. Other factors that affect the estimation are again low amplitude of the measured target responses and poor consistency of the pseudo forces for the frequency region between 0 and 150 Hz.

6 Conclusions

In this work an approach to FRF estimation for operating assemblies is proposed, where the source structure is characterized independently of the full assembly. Component-based TPA methods are exploited to describe

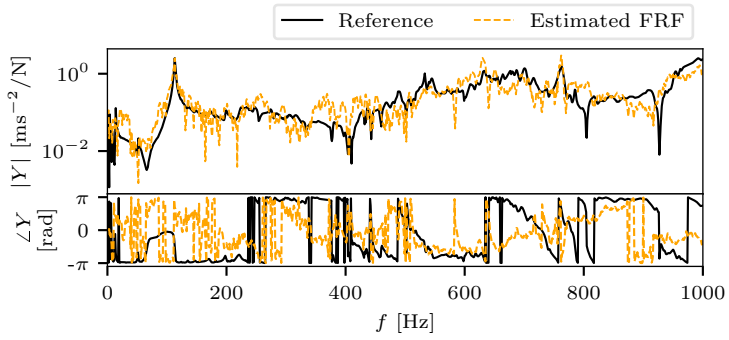

Figure 22: FRFs of the washing machine drum assembly for excitation $f_{\mathrm{ps},1}$ and response $\widetilde{u}_{3,3}$.

the source, and thus the forces, equivalent to the operational excitation, are valid for any assembly with a modified passive side. This transferability makes it possible to estimate the FRFs on the modified assemblies from equivalent or pseudo forces on the basis of a response measurement only, with the excitation force provided by the source itself.

The applicability of the proposed methodology is demonstrated through the numerical and experimental case studies. For this, the pseudo-force-based TPA method was used to characterize the source. Consistent FRFs are obtained for both the initial and modified assemblies, provided that a sufficient number of independent load cases at the source is available and that the pseudo forces are fully independent of the receiver side.

The approach is useful for cases when the dynamic properties of the assembly are required, but due to the complex geometry or mounting, the structure is inaccessible to excite at the source. Using dedicated laboratory test-benches for the source characterization, specifically designed to accommodate for the undemanding measurement campaign, arbitrary excitation locations can be easily accessed. Issues with a poor SNR can also be tackled if high response levels can be obtained while the structure is operating, but not when excited manually. Given that the equivalent forces are already determined by the source component provider, we can simply estimate any assembly's FRFs by measuring the target responses only.

Acknowledgements

The authors acknowledge partial financial support from the core research funding P2-0263 and the applied research project L2-1837, both financed by ARRS, the Slovenian research agency.

References

[1] D. de Klerk and C. Valentin, "Determination of an operating systems receptance frf data," in *Proceedings of the Twentyfifth International Modal Analysis Conference, Orlando, FL*, 2007.

[2] M. V. van der Seijs, D. de Klerk, and D. J. Rixen, "General framework for transfer path analysis: History, theory and classification of techniques," *Mechanical Systems and Signal Processing*, vol. 68, pp. 217–244, 2016.

[3] J. W. Verheij, "Multi-path sound transfer from resiliently mounted shipboard machinery: Experimental methods for analyzing and improving noise control," Ph.D. dissertation, TU Delft, Delft University of Technology, 1982.

[4] D. Lennström, M. Olsson, F. Wullens, and A. Nykänen, "Validation of the blocked force method for various boundary conditions for automotive source characterization," *Applied Acoustics*, vol. 102, pp. 108–119, 2016.

[5] M. V. van der Seijs, "Experimental dynamic substructuring: Analysis and design strategies for vehicle development," Ph.D. dissertation, Delft University of Technology, 2016.

[6] A. Moorhouse, A. Elliott, and T. Evans, "In situ measurement of the blocked force of structure-borne sound sources," *Journal of sound and vibration*, vol. 325, no. 4-5, pp. 679–685, 2009.

[7] M. Janssens and J. Verheij, "A pseudo-forces methodology to be used in characterization of structure-borne sound sources," *Applied Acoustics*, vol. 61, no. 3, pp. 285–308, 2000.

[8] J. Ortega Almirón, F. Bianciardi, P. Corbeels, and W. Desmet, "Predicting vibration levels on an experimental test case by using invariant loads (eg blocked forces) as source characterization," in *Proceedings of ISMA 2018-International Conference on Noise and Vibration Engineering and USD 2018-International Conference on Uncertainty in Structural Dynamics*. KU Leuven, 2018, pp. 4131–4145.

[9] M. Grialou, N. Totaro, J.-L. Guyader, and A. Bocquillet, "Characterization of surface impedance of vibro-acoustic subdomains with experimental measurements," *Journal of Sound and Vibration*, vol. 460, p. 114876, 2019.

[10] A. Moorhouse, T. Evans, and A. Elliott, "Some relationships for coupled structures and their application to measurement of structural dynamic properties in situ," *Mechanical Systems and Signal Processing*, vol. 25, no. 5, pp. 1574–1584, 2011.

[11] C. Höller and B. M. Gibbs, "Indirect determination of the mobility of structure-borne sound sources," *Journal of Sound and Vibration*, vol. 344, pp. 38–58, 2015.

[12] K. Wienen, M. Sturm, A. Moorhouse, and J. Meggitt, "Generalised round-trip identity—for the determination of structural dynamic properties at locations inaccessible or too distant for direct measurement," *Journal of Sound and Vibration*, vol. 511, p. 116325, 2021.

[13] T. Vrtač, "Karakterizacija modalnih parametrov pri obratovanju sistema z metodo pseudo sil," 2021. [Online]. Available: https://repozitorij.uni-lj.si/IzpisGradiva.php?lang=eng&id=129122

[14] N. Contartese, E. Nijman, and W. Desmet, "A procedure to restore measurement induced violations of reciprocity and passivity for frf-based substructuring," *Mechanical Systems and Signal Processing*, vol. 167, p. 108556, 2022.

[15] M. Haeussler, "Modular sound & vibration engineering by substructuring," Ph.D. dissertation, Universität München, 2021.

[16] T. Bregar, A. El Mahmoudi, M. Kodrič, D. Ocepek, F. Trainotti, M. Pogačar, M. Göldeli, G. Čepon, M. Boltežar, and D. J. Rixen, "pyfbs: A python package for frequency based substructuring," *Journal of Open Source Software*, vol. 7, no. 69, p. 3399, 2022.

[17] J. Meggitt and A. Moorhouse, "On the completeness of interface descriptions and the consistency of blocked forces obtained in situ," *Mechanical Systems and Signal Processing*, vol. 145, p. 106850, 2020.

[18] M. Haeussler, T. Mueller, E. Pasma, J. Freund, O. Westphal, and T. Voehringer, "Component tpa: Benefit of including rotational degrees of freedom and over-determination," in *Proceedings of the International Conference on Noise and Vibration Engineering, Leuven, Belgium*, 2020, pp. 7–9.

[19] M. Haeussler, D. Kobus, and D. Rixen, "Parametric design optimization of e-compressor nvh using blocked forces and substructuring," *Mechanical Systems and Signal Processing*, vol. 150, p. 107217, 2021.